

<https://doi.org/10.1038/s43247-024-01464-x>

Physical inconsistencies in the representation of the ocean heat-carbon nexus in simple climate models

Check for updates

Roland Séférian¹ ✉, Thomas Bossy^{2,3}, Thomas Gasser², Zebedee Nichols^{2,4}, Kalyn Dorheim⁵, Xuanming Su^{6,7}, Junichi Tsutsui⁸ & Yeray Santana-Falcón¹

The Ocean Heat–Carbon Nexus, linking ocean heat and carbon uptake, is crucial for understanding climate responses to cumulative carbon dioxide (CO₂) emissions and to net zero CO₂ emissions. It results from a suite of processes involving the exchange of heat and carbon across the sea–air interface as well as their storage below the mixed layer and redistribution by the ocean large-scale circulation. The Ocean Heat and Carbon Nexus is assumed to be consistently represented across two modelling platforms used in the latest IPCC assessments: the Earth System Models (ESMs) and the Simple Climate Models (SCMs). However, our research shows significant deficiencies in state-of-the-art SCMs in replicating the ocean heat–carbon nexus of ESMs due to a crude treatment of the ocean thermal and carbon cycle coupling. With one SCM, we show that a more realistic heat-to-carbon uptake ratio exacerbates the projected warming by 0.1 °C in low overshoot scenarios and up to 0.2 °C in high overshoot scenarios. It is therefore critical to explore how SCMs’ physical inconsistencies, such as the representation of the ocean heat–carbon nexus, can affect future warming projections used in climate assessments, not just by SCMs in Working Group 3 but also by ESMs in Working Group 1 via SCM-driven emission-to-concentration translation.

Atmospheric CO₂ continues to rise at unprecedented rates in response to human activities^{1,2}. The accumulation of CO₂ in the atmosphere prominently governs the increase in radiative forcing that drives in turn the addition of heat in the atmosphere^{3,4}.

In this global picture, the ocean plays a key role by slowing down the rate of atmospheric CO₂ accumulation and global warming.

On the one hand, the ocean absorbs more than 25% of anthropogenic CO₂ emissions annually^{1,2}, hence, exerting a strong control on the airborne fraction of CO₂ in the atmosphere.

On the other hand, the ocean absorbs about 90% of the additional heat resulting from the Earth energy imbalance induced by the accumulation of greenhouse gases in the atmosphere^{3–5}.

The interplay between the uptake of heat and carbon by the ocean is generally referred to as the “ocean heat–carbon nexus”¹.

By driving not only the accumulation of CO₂ and heat in the atmosphere but also the redistribution of heat and carbon within the global ocean across similar timescales, the ocean heat–carbon nexus exerts control on the response of the Earth’s climate and carbon cycle to cumulative CO₂ emissions (i.e., the transient climate response to cumulative CO₂ emissions¹, TCRE). In particular, the path independence of the TCRE emerges as a direct result of the interplay between the ocean heat and carbon uptake^{6–8}. The ocean heat–carbon nexus has also been shown as a critical geophysical property to explain the warming commitment to net zero emissions^{9,10}.

The ocean heat–carbon nexus arises from a well-understood combination of processes.

By governing the partitioning of the anthropogenic emission of CO₂ and additional heat, the exchange of heat and carbon across the sea–air interface emerges as the primary driver of the Nexus (e.g., refs. 1,3,5).

¹CNRM, Université de Toulouse, Météo-France, CNRS, Toulouse, France. ²International Institute for Applied Systems Analysis (IIASA), Laxenburg, Austria.

³Laboratoire des Sciences du Climat et de l’Environnement (LSCE), Gif-sur-Yvette, France. ⁴Melbourne Climate Futures, School of Geography, Earth and Atmospheric Sciences, The University of Melbourne, Melbourne, VIC, Australia. ⁵Joint Global Change Research Institute, Pacific Northwest National Laboratory, 5825 University Research Ct. #3500, College Park, MD, USA. ⁶Social Systems Division, National Institute for Environmental Studies (NIES), Tsukuba, Japan.

⁷Research Institute for Global Change/Research Center for Environmental Modelling and Application, Japan Agency for Marine–Earth Science and Technology (JAMSTEC), Yokohama, Japan. ⁸Sustainable System Research Laboratory, Central Research Institute of Electric Power Industry, Abiko, Japan.

✉ e-mail: roland.seferian@meteo.fr

This process is typically parameterized into well-established expressions that link the flux to wind stress and the gradient of heat or CO₂ across the sea-to-air interface¹¹.

The other driver of the ocean heat-carbon nexus arises from the suite of processes controlling the capacity of the ocean to store heat and CO₂, which are respectively governed by the strong heat capacity and the limited CO₂ buffering capacity of seawater¹². The large-scale redistribution of heat and carbon through the ocean circulation and mixing links these two quantities together over longer timescales^{5,13,14}.

Under rising atmospheric CO₂, the accumulated heat from a positive Earth energy imbalance is mainly stored in the ocean^{3,4}.

About 25% of the anthropogenic CO₂ emissions is absorbed by the ocean, leading to the accumulation of CO₂ in the uppermost layer of the ocean¹. The large-scale transport and mixing redistribute the accumulated heat and carbon across the ocean layers, linking together the uptake of heat and carbon with a near linear relationship (Fig. 1).

This near linear relationship breaks and takes the form of a regime shift^{1,15–17} (Fig. 1) with rising atmospheric CO₂ after which the uptake efficiency of the ocean for CO₂ reduces much faster than for the heat.

This regime shift arises from a combination of three factors.

First, both models and theory show that there is no physical limitation that would reduce the ability of surface ocean temperature to equilibrate with the atmospheric temperature. This implies that there is no mechanism that would limit the capacity of the ocean to take up the additional heat from the atmosphere^{5,18}.

Second, and in contrast, the capacity of the ocean to store CO₂ differs from its capacity to store heat because the carbon buffering capacity decreases as the ocean absorbs anthropogenic CO₂ and stores it as dissolved inorganic carbon^{12,19}. In addition, ocean warming reduces the solubility of CO₂ into seawater thus reducing the carbon sink efficiency^{16,17,20,21}.

Third, the accumulation of heat by the uppermost layers of the ocean reinforces the stratification of the surface ocean, slowing the mixing with the subsurface ocean of water masses in contact with the atmosphere^{15,19,20}. Together with salinity change, the subsequent changes in large-scale ocean circulation such as the Atlantic Meridional overturning circulation in response to global warming tends to exacerbate this phenomenon by slowing down the redistribution of heat and carbon within the global ocean^{13,14,18,22,23}. Together, the stratification and reduced mixing as well as the slowdown in major features of the ocean large-scale circulation reinforce the regime shift of the ocean heat-carbon nexus in a future warmer climate where each Joules taken up by the ocean will drive a stronger saturation of the ocean carbon uptake.

The wide diversity of geophysical climate models used in global in climate assessments such as IPCC^{24–26} are assumed to correctly model key features of the interplay between the ocean heat and carbon uptake¹⁵.

This diversity can be mapped in two main categories depending on their modeling paradigm.

The first category is the coupled climate models also known as the Earth system model (ESMs). This category of model represents a major tool

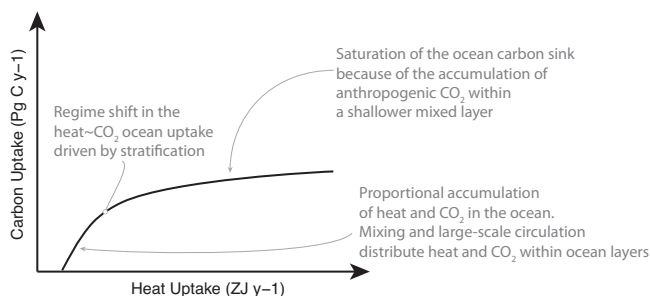


Fig. 1 | Depiction of the expected regime shift in the ocean heat-carbon nexus under rising atmospheric CO₂. The ocean heat-carbon nexus emerges from the relationship between the ocean heat uptake (*x* axis) and the ocean carbon uptake (*y* axis).

for IPCC Working Group (WG) I assessments. The modeling paradigm of ESMs primarily arise from the process understanding of the flow of energy, moisture, and chemicals through the atmosphere, ocean, and land surface, governing Earth's climate. In this model category, the representation of the suite of ocean processes that are involved in the uptake of heat and carbon by the ocean are included: most often explicitly resolved and sometimes parameterized. Through process representation, ESMs enable a wide range of interactions between the ocean and the other components of the Earth system²⁷. Of particular relevance, the modeling paradigm brings the representation of the ocean hydrodynamics and of the ocean carbon cycle on the same framework, ensuring that the large-scale transport of heat and carbon are directly linked^{13,14}. The latest generation of ESMs that have contributed to the 6th phase of the Coupled Model Intercomparison Project (CMIP6, ref. 28) describes these processes in unprecedented detail²⁴.

The second category is the Simple Climate Models (SCMs) that are based on a more diverse modeling paradigm than ESMs, and that emulate the response of most Earth system components through a suite of box models and impulse response functions^{29–36}. Therefore, their representation of ocean heat and carbon uptake follows their own modeling paradigm. Interactions between other components influencing the ocean heat and carbon cycle, such as sea ice are seldom directly modeled³⁷.

Yet, they are parametric models designed to be computing-efficient, flexible and easily tunable in order to emulate the response of complex ESMs within a certain domain of validity^{37,38}.

Thanks to their flexible framework, SCMs can account for multiple lines of evidence that counter known biases of the current generation of ESMs and hence resulting in better-constrained future projections^{39,40}. For the case of the ocean heat-carbon nexus, most SCMs include observational constraints on the historical global mean surface temperature but also on the ocean heat and carbon uptake⁴⁰. Because of these properties, SCMs have played a key role in the latest IPCC assessment in propagating the Working Group 1 (WG1) physical assessment²⁵ derived from ESMs to a wider array of emission pathways assessed by WG3²⁶. In addition, SCMs are not only used as the climate component of IPCC-class integrated assessment models that develop future emissions scenarios but also in the emission-to-concentration translation. This later use is of major importance because it feeds directly into the ESM framework for future climate projections⁴¹.

However, the question of how far the representation of the ocean heat-carbon nexus is comparable and physically consistent across the two modeling platforms has never been investigated.

Here, we use an ensemble of opportunity of state-of-the-art CMIP6 ESMs and SCMs that have participated in the Reduced Complexity Model Intercomparison Project (RCMIP, ref. 37) (see “Methods”) to track physical inconsistencies in the representation of the ocean heat-carbon nexus between these two class of climate models widely used in climate assessment. The objective of this work is threefold. We aim (1) to scrutinize how the coupling between ocean heat and carbon uptake is represented in these two modeling platforms, (2) to elaborate a mechanistic understanding in how the ocean heat-carbon cycle nexus is functioning in ESMs and SCMs, and (3) to shine light on deficiencies and potential for improvements.

Results and discussion

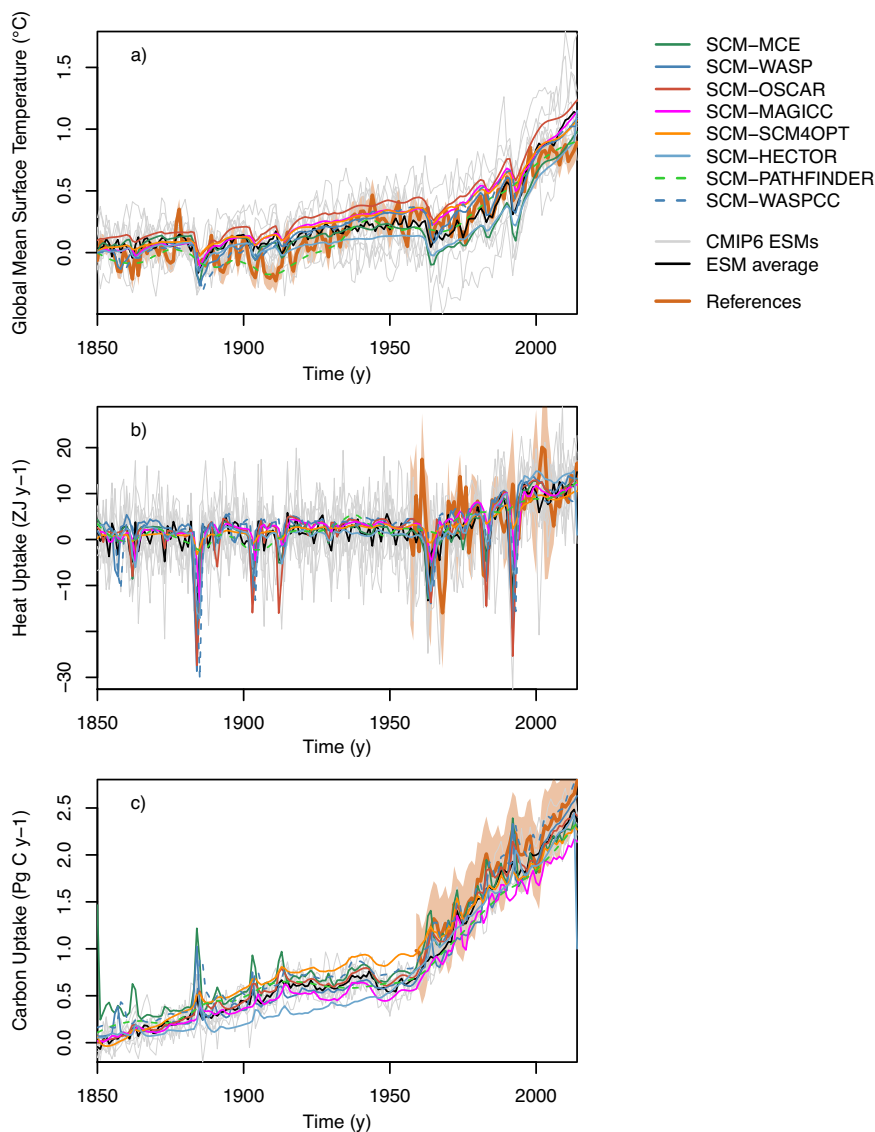
Comparison of key geophysical properties between ESMs and SCMs

Although based on a suite of assumptions and simplification, SCMs are fitted to reproduce key global features of the modern climate, as shown in Fig. 2.

Both ESMs and SCMs display good performance at replicating modern observations (Fig. 2 and Supplementary Table S1).

It is worth noting that the general agreement of ESMs with observations for global-scale metrics hide regional uncertainties that are documented in the scientific literature (e.g., refs. 8,9,16,22,42). These regional uncertainties are mostly related to the representation of ocean circulation and physics in ocean models that can impact future heat and carbon uptake

Fig. 2 | Performance of SCMs and ESMs at replicating historical observations. Comparison of the performance of SCMs and ESMs is assessed over the historical period (1850–2014) in terms of changes in **a** global mean surface temperature, **b** ocean heat uptake, and **c** ocean carbon uptake. The 1850–1900 period has been taken as a reference for changes in global mean surface temperature. The year 1850 has been taken as a reference for changes in ocean heat uptake and ocean carbon uptake. Observations are given in brown filled circles, individual ESMs in thin gray lines and ESM multi-model mean in black lines, SCMs that have contributed to RCMIP are given in solid colored lines. Newer models that did not (the upgraded version of WASP named WASPCC, and Pathfinder) are presented with dashed colored line. (see “Methods”). Global metrics for the references are estimated from the HadCRUT4 database⁵⁷ for global warming, the WOA-based ocean heat content⁴² and the ocean carbon sink from the Global Carbon project¹¹. These estimates are provided with a 1-sigma range of uncertainty.



efficiency^{16,22}. Models’ present-day stratification can modulate this response by acting on the background state of the ocean. Such regional dimension is missing from almost all SCMs (MAGICC has a hemispheric climate representation and OSCAR a regional land carbon cycle).

Interestingly, the agreement with the global observations is generally better for the SCMs thanks to their calibration on the observations or major climate features governing the response of the Earth system to anthropogenic and natural drivers^{39,40}. When comparing the performance of both modeling platforms at replicating modern observations, SCMs display a stronger correlation than ESMs for both global mean surface temperature (GMST) and ocean heat uptake (Supplementary Table S1). Both modeling platforms display comparable performance at capturing the recent evolution of the ocean carbon sink (Supplementary Table S1).

When used in an idealized simulation framework where atmospheric CO₂ rises by 1% per year, the responses of these two categories of models exhibit a much different picture (Fig. 3a).

Although the change in GMST is captured by both categories of models as documented in published climate sensitivity assessments¹³, the response of the ocean heat and carbon uptake as simulated by SCMs displays a much greater diversity than that of the ESMs (Fig. 3b, c).

The two ensembles of models diverge with rising CO₂. At 2×CO₂, solely the simulated GMST differs significantly between ESMs and SCMs (Table S2). At 4×CO₂ (Supplementary Table S2), the distribution of GMST, ocean heat, and carbon uptake as simulated by both modeling platforms

diverge significantly from each other. In addition, two SCMs (WASP and HECTOR) show an unexpected response to rising CO₂ by simulating a saturation of the heat uptake <10 ZJ y⁻¹ and a massive absorption of the CO₂ by the ocean >10 Pg C y⁻¹. An upgraded representation of the ocean carbon cycle in WASPCC improves the deficiency of the version of WASP that contributed to RCMIP. However, the representation of the ocean heat-carbon nexus by WASPCC is still far from replicating that of the ESMs ($R^2 \sim 0.3$).

Available perturbed parameter ensemble from MAGICC and Pathfinder SCMs (Supplementary Fig. S1) suggests that this feature is robust across a wide range of parameters and, hence, demonstrates that the representation of the ocean heat-carbon nexus arise prominently from the structural properties of SCMs.

The above-mentioned behavior results in a very different representation of the ocean heat-carbon nexus across the two categories of models (Fig. 3d), where ESMs capture a response closer to the theory than SCMs.

Interestingly, the response of both modeling platforms is hardly distinguishable with uptake in heat and carbon consistent in magnitude with those of the historical period (observed range, Fig. 3). This consistency in the response between the two modeling platforms can be explained by two factors. On the one hand, available historical observations do not provide a sufficient constraint to effectively calibrate SCMs for projecting in a warmer range. A similar assumption was made by ref. 43 highlighting the limits of historical record to constraint the climate sensitivity.

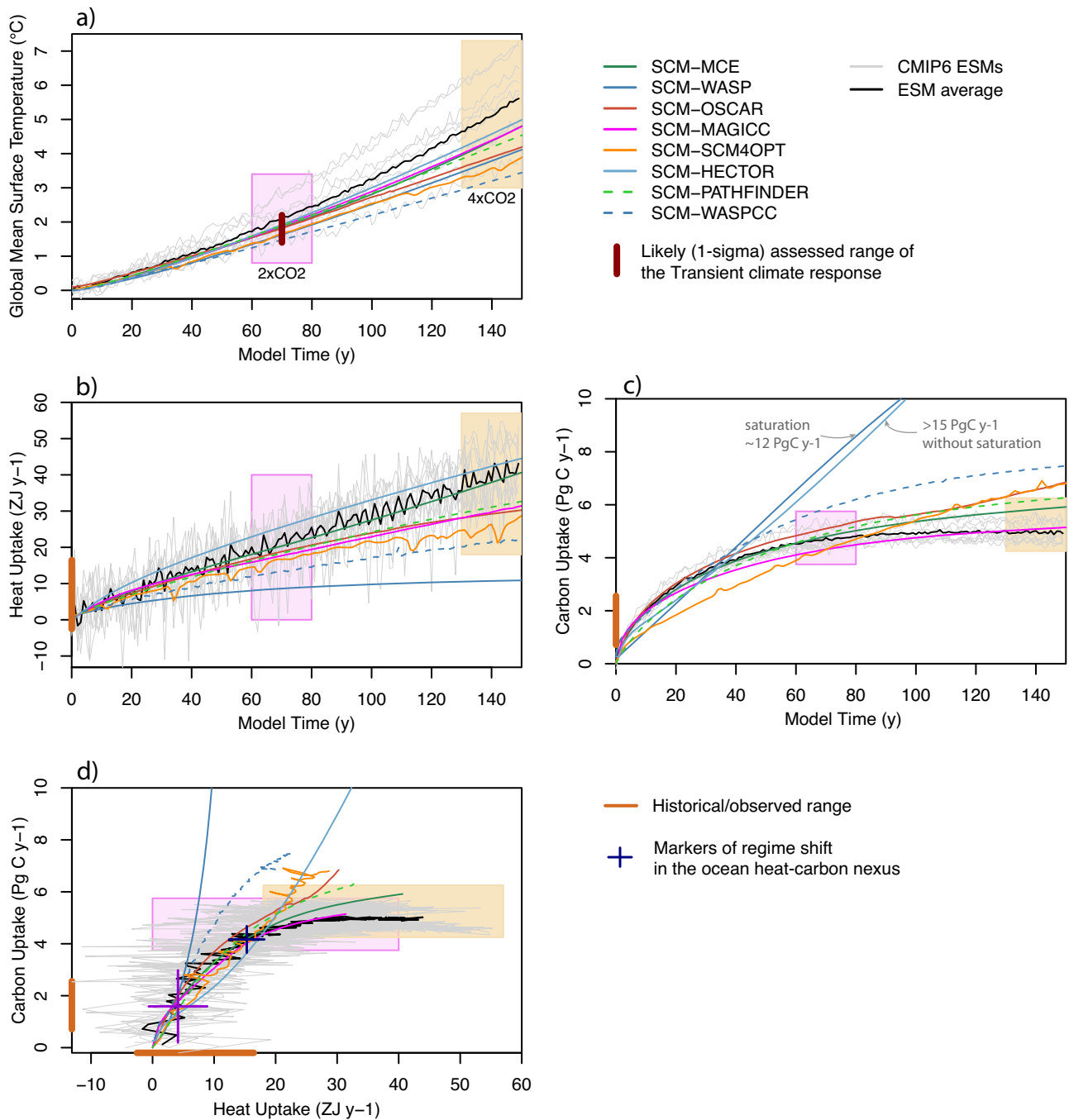


Fig. 3 | Comparison of projected warming and ocean heat-carbon nexus between ESMs and SCMs under an idealized set-up. **a–c** shows the temporal evolution of the projected warming, ocean heat uptake and ocean carbon uptake as simulated by both ESMs and SCMs. **d** displays the representation of the ocean heat-carbon nexus between ESMs and SCMs. SCMs are given in colored solid lines, individual ESMs in thin gray lines and ESM multi-model mean in black lines. Colored boxes highlight 20-year window centered around the year 70 and 140 where atmospheric CO₂ is

doubled (2×CO₂) and quadrupled (4×CO₂), respectively. The thick vertical red lines in **(a)** indicate the IPCC AR6 1-σ range for the transient climate response at CO₂ doubling³. **d** The magenta and black crosses represent the spread in ocean heat and carbon uptake at the time of the regime shift for SCMs and ESMs, respectively (see “Methods”). Solid colored lines are given for SCMs that have contributed to RCMIP, dashed colored lines are for two newer models that did not.

On the other hand, the response timescales of SCMs differ greatly from that of ESMs. Indeed, most SCMs poorly capture the regime shift in the ocean heat-carbon nexus. When tracking the timing of the regime shift in the ocean heat-carbon nexus as simulated by both modeling platforms (see “Methods”, Supplementary Figs. S2 and S3), all SCMs except MAGICC and Pathfinder show a change in the heat-carbon uptake relationship between three to seven years after the start of the simulation. The regime shift takes place much later in ESMs, that is, about 30 years

later than SCMs with a 1-σ range of 10 years (Supplementary Figs. S2 and S3).

Both the ocean heat and carbon uptakes respond to multiple drivers such as the change in ocean circulation, freshening due to change in precipitation patterns, sea ice melt, regional stratification, and operate under various timescales^{1,2}. Therefore, such an early shift raises questions on the realism of the timescales governing the large-scale transport of heat and carbon as emulated by the SCMs.

Inconsistent physical representation of the key driving mechanisms of the ocean heat-carbon nexus

We identify that the representation of the ocean heat-carbon nexus in SCMs suffers from physical inconsistencies in the representation of key driving mechanisms with respect to that of ESMs. These physical inconsistencies are underlain by many assumptions and simplifications employed in the modeling paradigm of most state-of-the-art SCMs.

A meta-analysis of the models' properties (Fig. 4a, b and Supplementary Table S3) shows that the modeling framework of SCMs treat the thermal response of the ocean to radiative forcing and that of the ocean carbon cycle to rising atmospheric CO₂ as two distinct modules (except for WASP and WASPCC). Therefore, a given SCM may rely on physically inconsistent structures and/or parameters—such as mixed-layer depths (MLD) and/or relaxation timescales—to simulate the ocean heat uptake or the ocean carbon uptake. It results in physical inconsistencies in the representation of the ocean Heat-Carbon nexus in SCMs. In contrast, ESMs consistently resolve the suite of processes governing the uptake of heat and carbon by the ocean.

Our meta-analysis highlights the absence or crude representation of the processes driving carbon and heat uptake such as the stratification or the

vertical transport (Fig. 4a, b and Supplementary Table S3). Indeed, most of the SCMs rely on pure-diffusion schemes for the vertical exchange of heat and carbon with the atmosphere. Only MAGICC accounts for a more comprehensive ocean scheme with a Diffusion–Upwelling–Entrainment algorithm³⁶, albeit solely for the heat.

On the coupling between ocean physics and carbon cycle, most SCMs rely on indirect interactions through climate-carbon cycle feedback parameters^{29–36} (Supplementary Table S3). That is, changes in the strength of ocean carbon sink is modulated changes in airborne fraction of atmospheric CO₂ and in the global mean surface temperature through carbon-concentration and carbon-climate feedbacks parameters. None of them involves ocean processes such as changes in ocean circulation, mixing, and changes in sea surface temperature patterns. Only OSCAR attempts to explicitly simulate the coupling between the thermal module and the carbon cycle module mimicking the impact of the ocean stratification on the ocean carbon uptake (Supplementary Fig. S3).

Our meta-analysis of the models' properties allows us also to scrutinize the representation of the ocean mixed-layer depth across the two modeling platforms. This field is an indirect proxy of ocean stratification. Interestingly, the mixed-layer depth is a model parameter for most SCMs, which is fixed in

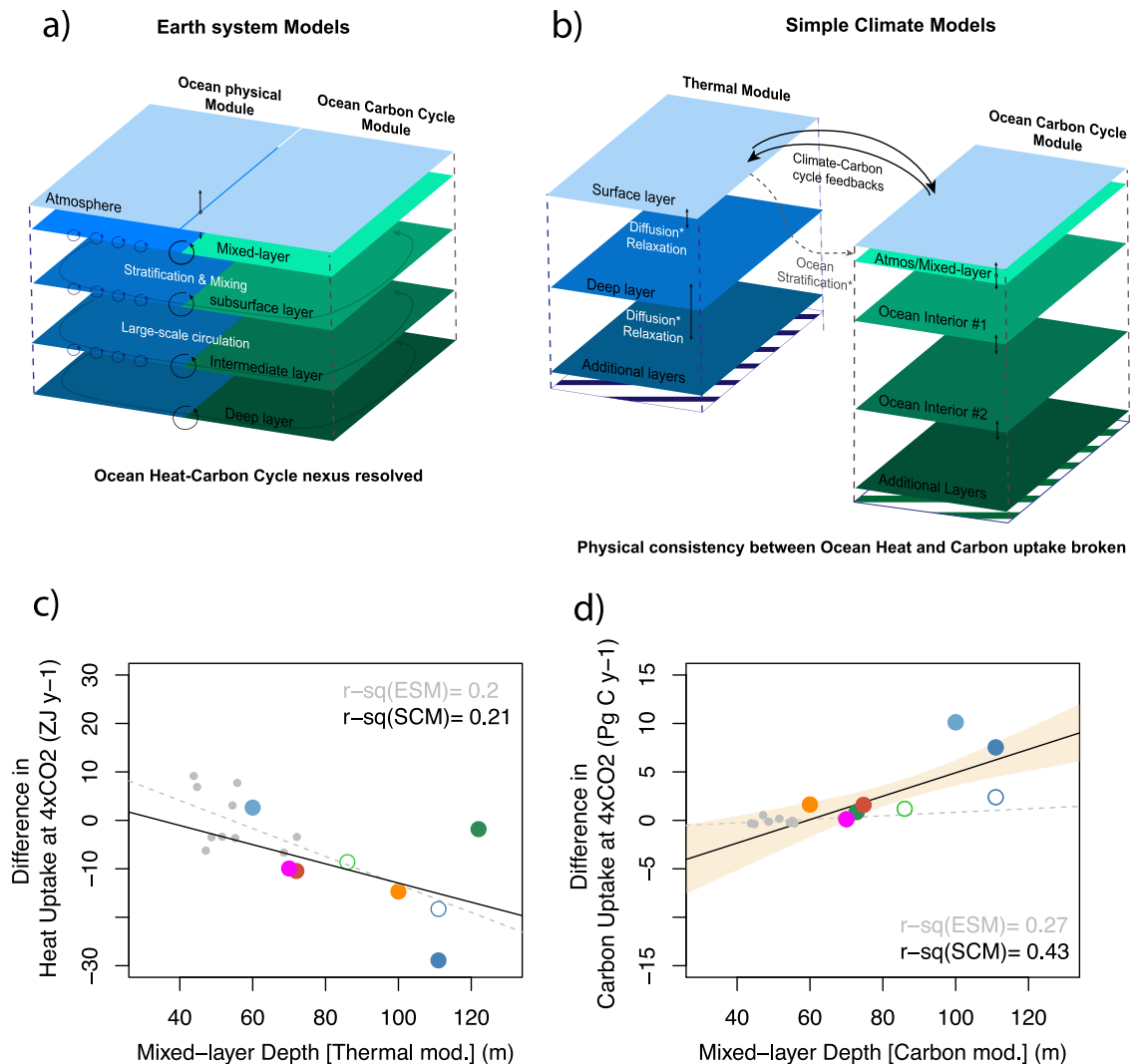


Fig. 4 | Structural and parametric model properties driving the representation of the ocean heat-carbon nexus within ESMs and SCMs. Top panels provide an overview of key structural modeling properties driving the representation of the ocean heat-carbon nexus within ESMs (a) and SCMs (b). Bottom panels shine light on key parametric differences between ESMs (gray points) and SCMs (colored

points) in the interplay between the mixed-layer depth and the ocean heat (c) and carbon uptake (d) at 4xCO₂ between the two categories of models. Colored points for SCMs are filled for the model versions that have contributed to RCMIP, colored circles are for two newer models that did not. Colors for SCMs is the same as for Figs. 1–3.

Table 1 | Maximum warming as predicted by Pathfinder with (left) and without (right) accounting for the ratio between heat and carbon uptake at $2\times\text{CO}_2$ of ESMs

	Peak warming (°C)			
	With constraints on the nexus		Without constraints on the nexus	
	Median	Range	Median	Range
ssp119	1.75	1.03–3.57	1.66	0.91–2.98
ssp126	2.06	1.14–3.52	1.94	1.03–3.57
ssp534-over	2.76	1.57–4.72	2.60	1.42–4.76
2100 warming (°C)				
	With constraints on the nexus		With constraints on the nexus	
ssp245	3.11	1.75–5.40	2.91	1.58–5.43
ssp370	4.35	2.52–7.47	4.07	2.28–7.52
ssp585	5.21	3.00–8.99	4.88	2.73–9.04

These estimates are based on the 2000-member perturbed parameter ensemble future projections of Pathfinder as shown in Supplementary Fig. S4. The maximum warming corresponds to the peak warming reached during the 21st century for the overshoot scenarios (ssp119, ssp126, and ssp534-over), whereas it corresponds to the warming reached in 2100 for the other scenarios (ssp245, ssp370, and ssp585).

time, whereas it is resolved in ESMs and hence responds to anthropogenic forcing (Supplementary Fig. S3).

Our analysis shows that, for all SCMs, the value of the global mean MLD falls outside the observational range, suggesting that this parameter has not been calibrated (Supplementary Fig. S3).

Because this feature is non-dynamically represented, SCMs fail at replicating this physical feature of the shoaling in mixed-layer depth with rising temperature^{44,45} as compared to ESMs that display a shoaling of the global mean MLD of ~ 20 m (much stronger in deep convection regions) at peak warming.

When tracking the role of the ocean mixed-layer depth in setting changes in ocean heat and carbon uptake (Fig. 4c, d), we show that the depth of the mixed-layer used in the ocean carbon module of SCMs has a stronger influence on the magnitude of the ocean carbon sink with a slope of $0.12 \text{ Pg C y}^{-1} \text{ m}^{-1}$ ($R^2 \sim 0.4$) than it does in ESMs with a slope of $0.01 \text{ Pg C y}^{-1} \text{ m}^{-1}$ ($R^2 \sim 0.3$).

This is not the case for the response of the ocean heat uptake, where SCMs simulate a response of $-0.2 \text{ ZJ y}^{-1} \text{ m}^{-1}$ ($R^2 \sim 0.2$) which is close to that of the ESMs ensemble with a slope of $-0.26 \text{ ZJ y}^{-1} \text{ m}^{-1}$ ($R^2 \sim 0.2$).

This small correlation between changes in ocean heat and carbon uptake, and mixed-layer depth in ESMs are not surprising because many others physical drivers, such as the redistribution of heat and carbon by the ocean circulation (e.g., refs. 8,9), can impact this relationship. On the contrary, the fact that SCMs exhibit a strong direct relationship emphasizes the inconsistency in the geophysical representation of the ocean heat-carbon nexus in such a modeling platform.

Together, these structural and parametric simplifications of ocean processes and relationships lead to a breakdown in a key mechanism of the ocean heat-carbon nexus responsible for the saturation of the ocean carbon sink.

Consequences for projections

We now investigate the impact of the representation of the ocean heat-carbon nexus in SCMs on future SSP-based projections^{46,47}. In particular, we use two high-mitigation/low-overshoot scenarios (ssp119 and ssp126), and one high-overshoot scenario (ssp534-over) for our analysis.

In order to get a traceable comparison, we bring the representation of the ocean heat-carbon nexus of the Pathfinder simple climate model⁴⁰ close to that simulated by the ESMs by constraining the relationship between the ocean heat uptake and the ocean carbon uptake at $2\times\text{CO}_2$ (see “Methods”).

Before applying such constraint, we find at peak warming ranges from 0.91°C to 2.98°C with a mean estimate of 1.66°C for ssp119, and from 1.03°C to 3.57°C with a mean estimate of 1.94°C for ssp126. The high-overshoot scenario (ssp534-over) displays a range of peak warming between 1.42°C and 4.76°C with a mean estimate of 2.60°C (Table 1).

The application of the geophysical constraint in the ocean heat-carbon nexus reinforced the simulated warming by about $+0.1^\circ\text{C}$ for both high-mitigation/low-overshoot scenarios and up to 0.2°C for the high-overshoot scenario (Table 1). Pathfinder simulates a mean warming of 1.75°C at peak warming in ssp119 and 2.06°C for ssp126. Under the high-overshoot scenario the peak warming reaches 2.76°C (Table 1). The constraint also results in a slightly smaller spread in projected warming, that is about 5–8% smaller with respect to the range of peak warming as simulated with the unconstrained version of Pathfinder (Table 1).

The temperature increase is markedly stronger ($>0.2^\circ\text{C}$ by 2100) in medium to high emission scenarios (Table 1, see also Supplementary Fig. S4) because both increases in Earth energy imbalance and in atmospheric CO_2 assumed in these scenarios speed up the occurrence of the regime shift in the ocean heat-carbon nexus. Through the geophysical constraints implemented in the model, Pathfinder captures the timing of the ocean stratification in response to increasing radiative forcing more consistently. Ocean stratification reinforces the accumulation of heat in the mixed layer and the atmosphere leading to exacerbate global warming with respect to the unconstrained version of Pathfinder.

While seemingly low, this 0.1°C difference is consequential in the case of ambitious low-warming scenarios. With an older version of the MAGICC simple climate model³⁶ with 600-probabilistic parameters samples, it was assessed that $+0.1^\circ\text{C}$ at peak warming reduces the likelihood of the ssp126 scenario to stay below 2°C from 66% to 54% and below 1.5°C from 10% to 6%. A similar feature is found for Pathfinder under ssp126 when considering the influence of an improved representation of the ocean heat-carbon nexus in the model on temperature outcomes (Supplementary Fig. S4).

A similar difference of 0.1°C in MAGICC temperature outcomes was also found in ref. 14 when comparing the IPCC SR15⁴⁸ and AR6⁴⁹ due to the increase in assessed historical warming between SR1.5 and AR6, and an improved (i.e., weaker) response to emissions. As stated in ref. 39, such difference is enough to cause all the “ 1.5°C no overshoot” scenarios to be reclassified as “ 1.5°C low overshoot” scenarios.

Here, for the recent categorization of scenarios⁵⁰ by the IPCC WGIII, this might be significant as the additional warming due to a more realistic representation of the ocean heat-carbon nexus could result in emptying the IPCC AR6 WGIII class of scenario⁵¹ limiting warming to 1.5°C ($>50\%$) with no or limited overshoot (i.e., C1 class composed of 97 scenarios).

However, despite suggesting a systematic structural bias in SCMs, further investigation is warranted, as our estimates here were obtained using only one model and without altering its structure (that is, Pathfinder remains with two distinct global ocean modules).

Finally, we also investigate the connection of the ocean heat-carbon nexus with the timing of the peak warming. As the timing of the ocean carbon uptake influences the temporal evolution of the airborne fraction of anthropogenic emissions, it exerts a direct control on the radiative forcing and, hence, on the peak warming. This mechanism takes place in all context but exerts a major control on the climate response after anthropogenic emissions are brought to zero (also known as the Zero Emission Commitment, refs. 6,7) or in overshoot scenarios⁵².

When comparing the timing of the peak uptake in carbon and heat by the ocean (Fig. 5), we show a noticeable difference between ESMs and SCMs. SCMs simulate a peak in carbon uptake several decades after the peak as simulated by ESM; implying a stronger uptake. A similar feature, although with a smaller amplitude, is found for the ocean heat uptake, for which the timing of SCMs lags several years behind that of ESMs.

Under such a controlled set-up where models are driven by concentration, we do not show a difference in the timing of projected peak warming across the two modeling platforms. However, when expanded to a

small ensemble of opportunity of emission-driven simulations (Supplementary Fig. S5), our findings suggest a noticeable difference in the timing of peak warming between the two modeling platforms, where projected warming of SCMs peaks several years ahead of that of ESMs. A similar feature has been highlighted by ref. 53 using the CESM2 Earth system model and a large perturbed parameter ensemble using the finite amplitude impulse response (FaIR) 1.3 simple climate model⁵⁴.

Conclusion

Using results of current generation ESMs and SCMs, this study provides insights into the impact of the representation of the ocean heat-carbon nexus on future state-of-the-art scenarios. We find that state-of-the-art SCMs have difficulties to replicate the ocean heat-carbon nexus of ESMs because of a crude treatment of the ocean thermal and carbon cycle coupling. This physical inconsistency of SCMs in the representation of the ocean heat-carbon nexus can have important consequences in future warming as modeled by the SCMs both in terms of magnitude and timing (Fig. 5).

We point out with Pathfinder SCM that a more realistic heat-to-carbon uptake ratio lead to exacerbate the projected warming by 0.1 °C in the low-overshoot scenarios and up to 0.2 °C in high-overshoot scenarios. Although small, this difference in projected warming is enough as to impact the scenario classification as well as the characterization of key geophysical properties of overshoots scenarios.

Taken together, these findings question the emission-to-concentration translation process achieved by SCMs within the framework of the Coupled Model Intercomparison project⁴¹. Our finding may argue, at minimum, the need to populate uncertainties in future CO₂ concentration and global temperature projections arising from SCMs geophysical assumptions, in addition to the well-known uncertainties resulting from the treatment of land-use land-cover change or lack thereof⁵⁵.

As SCMs are and will remain an important and easily actionable tool to assess environmental policy, it is key to improve where relevant the transfer of knowledge across modeling platforms in order to deliver the most robust estimates of future warming. Here, our work highlights that a largely overlooked component of this tool, the ocean heat-carbon nexus, may represent a potential for improving the geophysical consistency between models used in the scenario generation process and assessment.

Methods

Earth system models

This work exploits the results of 10 the current generation Earth System Models (ESMs) that have taken part in CMIP6²⁸. They are listed in Supplementary Table S3, and described in Supplementary Material. All simulations provide monthly outputs of surface air temperature (tas), ocean heat uptake (hfds) and ocean carbon fluxes (fgco2). All monthly gridded files were either averaged or integrated globally, and averaged at the yearly frequency. For the historical period, only the first available realization has been

considered in this work (the influence of multiple realization on the results is negligible).

Simple climate models

In this work we also used 8 available simple climate model (SCMs). All of these SCMs, except Pathfinder v1.0.1⁴⁰ and WASPCC have participated in the Reduced Complexity Model Intercomparison Project phase 1 (RCMIP1) (ref. 37), namely, Hector V3 alpha, MCE v1-1, MAGICC v7.5.3 as used in IPCC AR6 WG3, OSCAR v3.1.1 as used in IPCC AR6 WG1, SCM4OPT v3.0 and WASP v2.0. To be include in this work, SCMs must provide a breakdown between the land and the ocean carbon uptake. That is why a model such as the finite amplitude impulse response (FaIR) 1.3 simple climate model⁵⁵ is not included in this work.

In this phase, SCMs were assessed in terms of global mean temperature responses, comparing them to observations and to the response of ESMs. Pathfinder was assessed independently but following a comparable protocol.

Importantly, phase 1 of RCMIP requested that all models provide one set of simulations in which their equilibrium climate sensitivity (ECS) is set to 3 °C. As shown in ref. 37, setting the ECS to the same value across all SCMs removes a major cause of difference between SCMs that is not related to model structure. As such, this set-up is key to scrutinize the representation of the ocean heat-carbon nexus within SCM. The key characteristics of the 8 SCMs are described in the Supplementary Materials.

Simulations

This work exploits a wide array of simulations that are either part of CMIP6 (ref. 28) or RCMIP phase 1 (ref. 37). The historical simulation spans from 1850 to 2014 and then branches out into several future scenarios based on 6 shared socioeconomic pathways⁴⁶. Comparison of the key properties of the ocean heat-carbon nexus is conducted on an idealized simulation where CO₂ concentration rises up to quadrupling from its preindustrial level with a rate of 1% per year, the so-called 1pctco2 experiment.

The analysis of the timing of peak warming (Fig. 5) was conducted by branching a “reverse” simulation, where the CO₂ concentration declines back to its preindustrial level with a rate of 1% per year (the 1pctco2-cdr experiment). This simulation is part of the CDRMIP protocol⁵⁶.

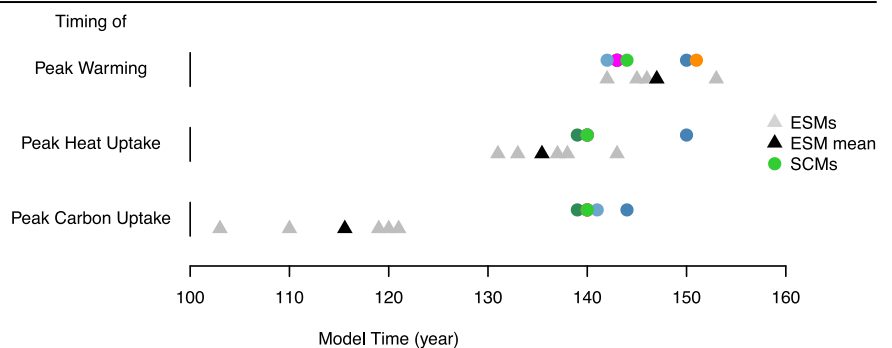
Tracking model structure

The key properties from the various SCMs mirroring ESMs features have been identified with the help of SCM modeling groups or developers to get further details on the ocean thermal and carbon modules, as well as the interplay between both modules. The key information on the 8 SCMs is gathered in the Supplementary materials (Supplementary Table S3).

Regime shift timing

In order to track objective measures of the regime shift in ocean heat-carbon nexus, we use a statistical linear model with a break-point at a given time

Fig. 5 | Peak warming, peak uptake of heat and carbon as simulated by SCMs and ESMs in an idealized overshoot simulation. Comparison of the timing of peak warming (top), peak heat uptake (middle) and peak carbon uptake (bottom) as simulated by SCMs and ESMs. SCMs are given in colored circles, individual ESMs in small gray triangles. The black triangle shows the timing of the ESM multi-model mean for each variable. Colors for SCMs is the same as for Figs. 1–3. The idealized overshoot simulation is obtained from the combination of the 1pctCO₂ and 1pctCO₂-cdr simulations where atmospheric CO₂ increase up to quadrupling from preindustrial level and then decrease with the same rate back to the initial state (“Methods”).



(Tshift). It can be written as follows:

$$\hat{OCU} = \alpha OHU + OCU_1 \quad \text{for } t \leq Tshift \quad (1)$$

$$\hat{OCU} = \beta OHU + OCU_2 \quad \text{for } t > Tshift \quad (2)$$

where \hat{OCU} is the least-squared fit of the ocean carbon uptake as function of the ocean heat uptake (OHU), α and OCU_1 are the regression slope and the intercept of the first linear segment and β and OCU_2 are the regression slope and the intercept of the second linear segment.

For each individual model, the timing of the “regime shift” is determined iteratively as a function of time in order to maximize the squared-correlation coefficient (R^2) for each of the statistical fits.

The R^2 time series is computed using this algorithm from individual model outputs.

However, ESMs and SCMs outputs cannot be compared directly because ESMs account for interannual variability whereas SCMs do not. Therefore, in order to minimize influence of the internal climate variability of the fits, ESM outputs were filtered with a LOESS filter with an equivalent degree of freedom of 4.35. Alternative smoothing approaches such as cubic splines were employed. They give comparable results for diagnosing the Tshift of each individual ESMs.

The estimate of Tshift is diagnosed from the R^2 time series when R^2 start decreasing linearly (see Supplementary Figs. S2 for ESMs and S3 for SCMs).

Multi-model estimates of Tshift are then used to compute ensemble means and $1-\sigma$ ranges for both modeling platforms as shown on Fig. 3.

The break points described here depends on the degree of saturation in the ocean carbon uptake. Consequently, the algorithm tracks the time at which the proportional relationship between the strength in ocean carbon uptake and the strength in the ocean heat uptake changes.

Correlation with the global mean mixed-layer depth

The role of the ocean mixed-layer depth in setting the ocean heat and carbon uptake (Fig. 4c, d) has been evaluated using the correlation between the deviation in ocean heat or carbon uptake with respect to the ESM multi-model mean at $4 \times \text{CO}_2$ and the global average mixed-layer depth as used by the thermal or carbon cycle module of SCMs, respectively. For ESMs, the same global average mixed-layer depth has been used for both correlation analyses.

Applying the ocean heat-carbon constraints in Pathfinder

In order to test the influence of the representation of the ocean heat-carbon uptake in SCM, we have employed Pathfinder v1.0.1⁴⁰. Pathfinder SCM is simple enough to be calibrated using Bayesian methods, which enables assimilation of the latest data from complex ESMs. In its current set-up, Pathfinder accounts for 19 geophysical constraints, none of them directly controls the ocean heat-carbon nexus.

To apply the ocean heat-carbon constraints in Pathfinder, we introduced a novel constraint built from ESM data using the ratio between the ocean heat and carbon uptake at $2 \times \text{CO}_2$ (year 70 of the 1pctco2 simulation). The distribution of this model-based constraint is assumed normal, and taken from the CMIP6 ESMs’ average and standard deviation. We integrate this novel constraint to the 19 others already used during the Bayesian calibration of Pathfinder. The main effect is to generate a correlation between the parameter reflecting the depth of the mixed layer and the parameters of the climate module.

Data availability

Earth system model outputs used in this work is based on standard outputs of the 6th phase of the Coupled Model Intercomparison Project. As such, all the files are available through the ESGF. SCMs output are part of the Reduced Complexity Model Intercomparison Project (RCMIP) and can be found here <https://www.rcmip.org/>. Global ocean and climate variables

from the 8 Simple Climate Models used in this study is available on <https://zenodo.org/records/11070854>.

Code availability

All code used in the current study is available from the corresponding author upon reasonable request.

Received: 4 October 2023; Accepted: 24 May 2024;

Published online: 01 June 2024

References

- Canadell, J. G. et al. Global carbon and other biogeochemical cycles and feedbacks. In *Climate Change 2021: The Physical Science Basis. Contribution of Working Group I to the Sixth Assessment Report of the Intergovernmental Panel on Climate Change* (eds Masson-Delmotte, V. et al.) 673–816 (Cambridge University Press, Cambridge, United Kingdom and New York, 2021).
- Friedlingstein, P. et al. Global carbon budget 2022. *Earth Syst. Sci. Data* **14**, 4811–4900 (2022).
- Forster, P. et al. The Earth’s energy budget, climate feedbacks, and climate sensitivity. In *Climate Change 2021: The Physical Science Basis. Contribution of Working Group I to the Sixth Assessment Report of the Intergovernmental Panel on Climate Change* (eds Masson-Delmotte, V. et al.) 923–1054 (Cambridge University Press, Cambridge, United Kingdom and New York, 2021).
- vonSchuckmann, K. et al. Heat stored in the Earth system 1960–2020: where does the energy go? *Earth Syst. Sci. Data* **15**, 1675–1709 (2023).
- Fox-Kemper, B. et al. Ocean, cryosphere and sea level change. In *Climate Change 2021: The Physical Science Basis. Contribution of Working Group I to the Sixth Assessment Report of the Intergovernmental Panel on Climate Change* (eds Masson-Delmotte, V. et al.) 1211–1362 (Cambridge University Press, Cambridge, United Kingdom and New York, 2021).
- MacDougall, A. H. The oceanic origin of path-independent carbon budgets. *Sci. Rep.* **7**, 10373 (2017).
- MacDougall, A. H. & Friedlingstein, P. The origin and limits of the near proportionality between climate warming and cumulative CO_2 emissions. *J. Climate* **28**, 4217–4230 (2015).
- Williams, R. G., Goodwin, P., Roussenov, V. M. & Bopp, L. A framework to understand the transient climate response to emissions. *Environ. Res. Lett.* **11**, 015003 (2016).
- MacDougall, A. H. et al. Is there warming in the pipeline? A multi-model analysis of the Zero Emissions Commitment from CO_2 . *Biogeosciences* **17**, 2987–3016 (2020).
- Palazzo Corner, S. et al. The Zero Emissions Commitment and climate stabilization. *Front. Sci.* **1**, 1170744 (2023).
- Garbe, C. S. et al. Transfer across the air-sea interface. In *Ocean-Atmosphere Interactions of Gases and Particles* (eds Liss, P. S. & Johnson, M. T.) 56–112 (Springer, Berlin, Heidelberg, 2014).
- Egleston, E. S., Sabine, C. L. & Morel, F. M. M. Revelle revisited: buffer factors that quantify the response of ocean chemistry to changes in DIC and alkalinity. *Glob. Biogeochem. Cycles* **24**, GB1002 (2010).
- Frölicher, T. L. et al. Dominance of the southern ocean in anthropogenic carbon and heat uptake in CMIP5 models. *J. Clim.* **28**, 862–886 (2015).
- Williams, R. G., Katavouta, A. & Roussenov, V. Regional asymmetries in ocean heat and carbon storage due to dynamic redistribution in climate model projections. *J. Clim.* **34**, 3907–3925 (2021).
- Bourgeois, T. et al. Stratification constrains future heat and carbon uptake in the Southern Ocean between 30°S and 55°S. *Nat. Commun.* **13**, 340 (2022).
- Schwinger, J. et al. Nonlinearity of ocean carbon cycle feedbacks in CMIP5 earth system models. *J. Clim.* **27**, 3869–3888 (2014).

17. Arora, V. K. et al. Carbon-concentration and carbon-climate feedbacks in CMIP6 models and their comparison to CMIP5 models. *Biogeosciences* **17**, 4173–4222 (2020).
18. Li, Z., England, M. H. & Groeskamp, S. Recent acceleration in global ocean heat accumulation by mode and intermediate waters. *Nat. Commun.* **14**, 6888 (2023).
19. Chikamoto, M. O., DiNezio, P. & Lovenduski, N. Long-term slowdown of ocean carbon uptake by alkalinity dynamics. *Geophys. Res. Lett.* **50**, e2022GL101954 (2023).
20. Séférian, R., Iudicone, D., Bopp, L., Roy, T. & Madec, G. Water mass analysis of effect of climate change on air–sea CO₂ fluxes: the Southern Ocean. *J. Clim.* **25**, 3894–3908 (2012).
21. Terhaar, J., Frölicher, T. L. & Joos, F. Observation-constrained estimates of the global ocean carbon sink from Earth system models. *Biogeosciences* **19**, 4431–4457 (2022).
22. Winton, M., Takahashi, K. & Held, I. M. Importance of ocean heat uptake efficacy to transient climate change. *J. Clim.* **23**, 2333–2344 (2010).
23. Winton, M., Griffies, S. M., Samuels, B. L., Sarmiento, J. L. & Frölicher, T. L. Connecting changing ocean circulation with changing climate. *J. Clim.* **26**, 2268–2278 (2013).
24. IPCC: Annex II: Models [Gutiérrez, J. M., A.-M. Tréguier (eds.)]. In *Climate Change 2021: The Physical Science Basis. Contribution of Working Group I to the Sixth Assessment Report of the Intergovernmental Panel on Climate Change* (eds Masson-Delmotte, V. et al.) 2087–2138 (Cambridge University Press, Cambridge, United Kingdom and New York, 2021).
25. IPCC, 2021: Summary for Policymakers. In: *Climate Change 2021: The Physical Science Basis. Contribution of Working Group I to the Sixth Assessment Report of the Intergovernmental Panel on Climate Change*. (eds Masson-Delmotte, V. et al.) pp. 3–32 (Cambridge University Press, Cambridge, United Kingdom and New York, NY, USA, 2021) <https://doi.org/10.1017/9781009157896.001>.
26. IPCC: summary for policymakers. In *Climate Change 2022: Mitigation of Climate Change. Contribution of Working Group III to the Sixth Assessment Report of the Intergovernmental Panel on Climate Change* (eds Shukla, P. R. et al.) (Cambridge University Press, Cambridge, UK and New York, NY, USA, 2022) <https://doi.org/10.1017/9781009157926.001>.
27. Séférian, R. et al. Tracking improvement in simulated marine biogeochemistry between CMIP5 and CMIP6. *Curr. Clim. Change Rep.* **6**, 95–119 (2020).
28. Eyring, V. et al. Overview of the Coupled Model Intercomparison Project Phase 6 (CMIP6) experimental design and organization. *Geosci. Model Dev.* **9**, 1937–1958 (2016).
29. Hartin, C. A., Patel, P., Schwarber, A., Link, R. P. & Bond-Lamberty, B. P. A simple object-oriented and open-source model for scientific and policy analyses of the global climate system—Hector v1.0. *Geosci. Model Dev.* **8**, 939–955 (2015).
30. Kriegler, E. *Imprecise Probability Analysis for Integrated Assessment of Climate Change*. Doctoral thesis, Universität Potsdam (2005).
31. Su, X., Tachiiri, K., Tanaka, K., Watanabe, M. & Kawamiya, M. Identifying crucial emission sources under low forcing scenarios by a comprehensive attribution analysis. *One Earth* **5**, 1–13 (2022).
32. Tanaka, K. et al. Aggregated carbon cycle, atmospheric chemistry and climate model (ACC2): description of forward and inverse mode. https://pure.mpg.de/rest/items/item_994422/component/file_994421/content (2007).
33. Tsutsui, J. Minimal CMIP Emulator (MCE v1.2): a new simplified method for probabilistic climate projections. *Geosci. Model Dev.* **15**, 951–970 (2022).
34. Gasser, T. et al. The compact Earth system model OSCAR v2.2: description and first results. *Geosci. Model Dev.* **10**, 271–319 (2017).
35. Goodwin, P. How historic simulation-observation discrepancy affects future warming projections in a very large model ensemble. *Clim. Dyn.* CLDY-D-15-00368R2, <https://doi.org/10.1007/s00382-015-2960-z> (2016).
36. Meinshausen, M., Raper, S. C. B. & Wigley, T. M. L. Emulating coupled atmosphere-ocean and carbon cycle models with a simpler model, MAGICC6—Part 1: model description and calibration. *Atmos. Chem. Phys.* **11**, 1417–1456 (2011).
37. Nicholls, Z. R. J. et al. Reduced Complexity Model Intercomparison Project Phase 1: introduction and evaluation of global-mean temperature response. *Geosci. Model Dev.* **13**, 5175–5190 (2020).
38. Nicholls, Z. et al. Reduced complexity Model Intercomparison Project Phase 2: synthesizing Earth system knowledge for probabilistic climate projections. *Earth's Future* **9**, e2020EF001900 (2021).
39. Nicholls, Z. et al. Changes in IPCC scenario assessment emulators between SR1.5 and AR6 unraveled. *Geophys. Res. Lett.* **49**, e2022GL099788 (2022).
40. Bossy, T., Gasser, T. & Ciais, P. Pathfinder v1.0.1: a Bayesian-inferred simple carbon–climate model to explore climate change scenarios. *Geosci. Model Dev.* **15**, 8831–8868 (2022).
41. Meinshausen, M. et al. The shared socio-economic pathway (SSP) greenhouse gas concentrations and their extensions to 2500. *Geosci. Model Dev.* **13**, 3571–3605 (2020).
42. Kuhlbrodt, T., Voldoire, A., Palmer, M. D., Geoffroy, O. & Killick, R. E. Historical ocean heat uptake in two pairs of CMIP6 models: global and regional perspectives. *J. Clim.* **36**, 2183–2203 (2023).
43. Sherwood, S. C. et al. An assessment of Earth's climate sensitivity using multiple lines of evidence. *Rev. Geophys.* **58**, e2019RG000678 (2020).
44. Sallée, J. B. et al. Summertime increases in upper-ocean stratification and mixed-layer depth. *Nature* **591**, 592–598 (2021).
45. Treguier, A. M. et al. The mixed-layer depth in the Ocean Model Intercomparison Project (OMIP): impact of resolving mesoscale eddies. *Geosci. Model Dev.* **16**, 3849–3872 (2023).
46. O'Neill, B. C. et al. The Scenario Model Intercomparison Project (ScenarioMIP) for CMIP6. *Geosci. Model Dev.* **9**, 3461–3482 (2016).
47. Tebaldi, C. et al. Climate model projections from the scenario model intercomparison project (scenariomip) of CMIP6. *Earth Syst. Dyn.* **12**, 253–293 (2021).
48. Rogelj, J. et al. Mitigation pathways compatible with 1.5 °C in the context of sustainable development (eds). In *Global Warming of 1.5 °C: An IPCC Special Report on The Impacts of Global Warming of 1.5 °C Above Pre-industrial Levels and Related Global Greenhouse Gas Emission Pathways, in the Context Of Strengthening The Global Response to The Threat of Climate Change, Sustainable Development, and Efforts to Eradicate Poverty*. (World Meteorological Organization, 2018).
49. Riahi, K. et al. (eds). In *IPCC, 2022: Climate Change 2022: Mitigation of Climate Change Contribution of Working Group III to the Sixth Assessment Report of the Intergovernmental Panel on Climate Change (chap. 3)* (Cambridge University Press, 2022).
50. Schleussner, C. F. et al. An emission pathway classification reflecting the Paris Agreement climate objectives. *Commun. Earth Environ.* **3**, 135 (2022).
51. Pathak, M. et al. Technical Summary. In *Climate Change 2022: Mitigation of Climate Change. Contribution of Working Group III to the Sixth Assessment Report of the Intergovernmental Panel on Climate Change* (eds Shukla, P. R. et al.) (Cambridge University Press, Cambridge, UK and New York, NY, USA, 2022) <https://doi.org/10.1017/9781009157926.002>.
52. Koven, C. D. et al. Multi-century dynamics of the climate and carbon cycle under both high and net negative emissions scenarios. *Earth Syst. Dyn.* **13**, 885–909 (2022).
53. Koven, C. D., Sanderson, B. M. & Swann, A. L. S. Much of zero emissions commitment occurs before reaching net zero emissions. *Environ. Res. Lett.* **18**, 14017 (2023).

54. Smith, C. J. et al. FAIR v1. 3: a simple emissions-based impulse response and carbon cycle model. *Geosci. Model Dev.* **11**, 2273–2297 (2018).
55. Melnikova, I. et al. Impact of bioenergy crop expansion on climate–carbon cycle feedbacks in overshoot scenarios. *Earth Syst. Dyn.* **13**, 779–794 (2022).
56. Keller, D. P. et al. The Carbon Dioxide Removal Model Intercomparison Project (CDRMIP): rationale and experimental protocol for CMIP6. *Geosci. Model Dev.* **11**, 1133–1160 (2018).
57. Morice, C. P., Kennedy, J. J., Rayner, N. A. & Jones, P. D. Quantifying uncertainties in global and regional temperature change using an ensemble of observational estimates: the HadCRUT4 data set. *J. Geophys. Res. Atmos.* **117**, D08101 (2012).

Acknowledgements

R.S., T.G., T.B., Y.S.-F., and Z.N. received support from the European Union's Horizon 2020 research and innovation programme under Grant Agreement N° 101003536 (ESM2025 – Earth System Models for the Future). R.S. also acknowledges funding from the European Union's Horizon Europe research and innovation programme under OptimESM (grant agreement No 101081193). X.S. received support from the Program for the Advanced Studies of Climate Change Projection (SENTAN, Grant Number JPMXD0722681344) from the Ministry of Education, Culture, Sports, Science and Technology (MEXT), Japan, and the Decarbonized and Sustainable Society Research Program at the National Institute for Environmental Studies, Japan. This study has also received funding from Agence Nationale de la Recherche - France 2030 as part of the PEPR TRACCS programme under grant number ANR-22-EXTR-0008 and ANR-22-EXTR-0009.

Author contributions

R.S. conceived the study, performed the analysis and wrote the manuscript with contribution of T.B., T.G., Y.S.-F., Z.N., K.D., X.S., and J.T., T.G., and T.B. performed additional simulations with the Pathfinder SCM.

Competing interests

The authors declare no competing interests.

Additional information

Supplementary information The online version contains supplementary material available at <https://doi.org/10.1038/s43247-024-01464-x>.

Correspondence and requests for materials should be addressed to Roland Séférian.

Peer review information *Communications Earth & Environment* thanks Fabrice Lacroix and the other, anonymous, reviewer(s) for their contribution to the peer review of this work. Primary Handling Editors: Prof Regina Rodrigues, Dr Clare Davis, and Dr Alice Drinkwater. A peer review file is available.

Reprints and permissions information is available at <http://www.nature.com/reprints>

Publisher's note Springer Nature remains neutral with regard to jurisdictional claims in published maps and institutional affiliations.

Open Access This article is licensed under a Creative Commons Attribution 4.0 International License, which permits use, sharing, adaptation, distribution and reproduction in any medium or format, as long as you give appropriate credit to the original author(s) and the source, provide a link to the Creative Commons licence, and indicate if changes were made. The images or other third party material in this article are included in the article's Creative Commons licence, unless indicated otherwise in a credit line to the material. If material is not included in the article's Creative Commons licence and your intended use is not permitted by statutory regulation or exceeds the permitted use, you will need to obtain permission directly from the copyright holder. To view a copy of this licence, visit <http://creativecommons.org/licenses/by/4.0/>.

© The Author(s) 2024